

## Article

---

# The St. Benedict Facility: Probing Fundamental Symmetries through Mixed Mirror $\beta$ -Decays

---

William S. Porter, Daniel W. Bardayan, Maxime Brodeur, Daniel P. Burdette, Jason A. Clark, Aaron T. Gallant, Alicen M. Houff, James J. Kolata, Biying Liu, Patrick D. O'Malley et al.

## Special Issue

Advances in Ion Trapping of Radioactive Ions

Edited by

Dr. Maxime Brodeur

## Article

# The St. Benedict Facility: Probing Fundamental Symmetries through Mixed Mirror $\beta$ -Decays

William S. Porter <sup>1,\*</sup>, Daniel W. Bardayan <sup>1</sup>, Maxime Brodeur <sup>1</sup>, Daniel P. Burdette <sup>2</sup>, Jason A. Clark <sup>2,3</sup>, Aaron T. Gallant <sup>4</sup>, Alicen M. Houff <sup>1</sup>, James J. Kolata <sup>1</sup>, Biying Liu <sup>1,2</sup>, Patrick D. O’Malley <sup>1</sup>, Caleb Quick <sup>1</sup>, Fabio Rivero <sup>1</sup>, Guy Savard <sup>2,5</sup>, Adrian A. Valverde <sup>2</sup> and Regan Zite <sup>1</sup>

<sup>1</sup> Department of Physics and Astronomy, University of Notre Dame, Notre Dame, IN 46556, USA

<sup>2</sup> Physics Division, Argonne National Laboratory, Lemont, IL 60439, USA

<sup>3</sup> Department of Physics and Astronomy, University of Manitoba, Winnipeg, MB R3T 2N2, Canada

<sup>4</sup> Nuclear and Chemical Sciences Division, Lawrence Livermore National Laboratory, Livermore, CA 94550, USA

<sup>5</sup> Department of Physics, University of Chicago, Chicago, IL 60637, USA

\* Correspondence: wporter@nd.edu

**Abstract:** Precise measurements of nuclear beta decays provide a unique insight into the Standard Model due to their connection to the electroweak interaction. These decays help constrain the unitarity or non-unitarity of the Cabibbo–Kobayashi–Maskawa (CKM) quark mixing matrix, and can uniquely probe the existence of exotic scalar or tensor currents. Of these decays, superallowed mixed mirror transitions have been the least well-studied, in part due to the absence of data on their Fermi to Gamow–Teller mixing ratios ( $\rho$ ). At the Nuclear Science Laboratory (NSL) at the University of Notre Dame, the Superallowed Transition Beta–Neutrino Decay Ion Coincidence Trap (St. Benedict) is being constructed to determine the  $\rho$  for various mirror decays via a measurement of the beta–neutrino angular correlation parameter ( $a_{\beta\nu}$ ) to a relative precision of 0.5%. In this work, we present an overview of the St. Benedict facility and the impact it will have on various Beyond the Standard Model studies, including an expanded sensitivity study of  $\rho$  for various mirror nuclei accessible to the facility. A feasibility evaluation is also presented that indicates the measurement goals for many mirror nuclei, which are currently attainable in a week of radioactive beam delivery at the NSL.



**Citation:** Porter, W.S.; Bardayan, D.W.; Brodeur, M.; Burdette, D.P.; Clark, J.A.; Gallant, A.T.; Houff, A.M.; Kolata, J.J.; Liu, B.; O’Malley, P.D.; et al. The St. Benedict Facility: Probing Fundamental Symmetries through Mixed Mirror  $\beta$ -Decays. *Atoms* **2023**, *11*, 129. <https://doi.org/10.3390/atoms11100129>

Academic Editor: Elmar Träbert

Received: 30 August 2023

Revised: 26 September 2023

Accepted: 9 October 2023

Published: 11 October 2023



**Copyright:** © 2023 by the authors. Licensee MDPI, Basel, Switzerland. This article is an open access article distributed under the terms and conditions of the Creative Commons Attribution (CC BY) license (<https://creativecommons.org/licenses/by/4.0/>).

## 1. Introduction

An understanding of the universe at the most fundamental level has long been an aim of the physics community. The Standard Model stands as the most complete fundamental description of matter and its interactions, yet many phenomena, including the matter–antimatter asymmetry, gravitational interaction, and the neutrino mass [1], are not well-described within the current framework. This has prompted widespread efforts to search for physics beyond the Standard Model (BSM), which would simultaneously show an inconsistency with the current Standard Model picture while also potentially giving credence to one of many proposed theoretical alternatives [2]. While high-energy physicists approach this task by pushing our acceleration capabilities to higher and higher energies and intensities, nuclear physicists have elected to push the precision frontiers at low energies to constrain the Standard Model via precision measurements of nuclear observables, particularly those associated with nuclear beta decay [3].

One of the strongest constraints beta decay observables provided is on the Cabibbo–Kobayashi–Maskawa (CKM) quark mixing matrix, which describes the mismatch between a quark’s mass and weak eigenstates [4]. Completeness of the Standard Model would imply

this matrix is unitary, and thus any deviation would indicate BSM physics [5]. The most precise unitarity test comes from the matrix elements involving the up quark, given as:

$$\sum_i |V_{ui}|^2 = |V_{ud}|^2 + |V_{us}|^2 + |V_{ub}|^2 = 1, \quad (1)$$

where the two smaller elements,  $V_{us}$  and  $V_{ub}$  are determined from kaon decays [6] and semileptonic B hadron decays [7], respectively. The highest precision results currently yield a  $2.4\sigma$  deviation from unitarity [8], calculated with  $V_{ud} = 0.97373(31)$ ,  $V_{us} = 0.2243(5)$ , and  $V_{ub} = 0.00394(36)$ . All elements cannot be determined directly from first principles, but they can be determined experimentally. The largest element,  $V_{ud}$ , can be determined via one of four different methods. The first two of these involve the decay of single hadrons, the pion and neutron, which are simple systems of up and down quarks and/or anti-quarks, and thus offer a direct approach to  $V_{ud}$  determination without the need to consider complex nuclear interactions. Pion decay determination, however, is severely statistics-limited by a low branching ratio of  $10^{-8}$  [9]. Additionally, neutron decay determination is plagued by a disagreement in the neutron lifetime on the order of  $4\sigma$  by the two primary measurement techniques [10].

The other two measurement methods involve the beta decays of multi-nucleon systems, which, though accompanied by the added complexity of nuclear interactions, are a more readily-accessible higher-statistics system available for study. Additionally, these transitions rely on the determination of several  $f_{Vt}$ -values to extract a value for  $V_{ud}$ , which provides a statistical advantage. Of these two, superallowed pure Fermi decays, which occur between  $0^+$  nuclear states, offer the most precise determination of  $V_{ud}$  mentioned above, with a relative uncertainty of  $\sim 3.1 \times 10^{-4}$  [8].

While superallowed pure Fermi transitions currently provide the most precise  $V_{ud}$  determination, interest in the less well-studied superallowed mixed mirror transitions, which occur between half-integer spin states, is growing, as they form a separate ensemble of nuclei that can be used to test the accuracy of the obtained  $V_{ud}$  value [11]. Determination of  $V_{ud}$  from mirror nuclear beta decays is similar to that of their pure Fermi brethren, but must also include a Gamow–Teller component alongside the Fermi one to account for the two available decay modes. This results in the addition of the Fermi to Gamow–Teller mixing ratio ( $\rho$ ) to the  $f_{Vt}$ -value equation, given as:

$$f_{Vt}(1 + \delta_R)(1 + \delta_{NS} - \delta_C) = \frac{K}{2G_F^2 V_{ud}^2 (1 + \Delta_R)(1 + \frac{f_A}{f_V} \rho)}, \quad (2)$$

where  $f_{Vt}$  is the comparative half-life,  $K$  and  $G_F$  are constants,  $f_A$  and  $f_V$  are the statistical rate functions from the axial–vector and vector interactions for the two decay modes [12], and the various  $\delta$  and  $\Delta$  terms are theoretical corrections [13].  $f_{Vt}$  is determined through experimental measurements of precise total transition energies ( $Q_{EC}$ -values), half-lives ( $t_{1/2}$ ), and branching ratios (BR). The current value for  $V_{ud}$  from mixed mirror decays agrees with unitarity within  $1\sigma$  while also agreeing with the pure Fermi value, as shown in Figure 1. The mixed decay value uncertainty, however, is three times larger than the pure Fermi value [14], as the needed quantities have only been measured for a few transitions. More experimental data from mirror decays is needed to increase the precision of the extracted value of  $V_{ud}$  and confirm (or not) the observed tension with unitarity seen with pure Fermi transitions.

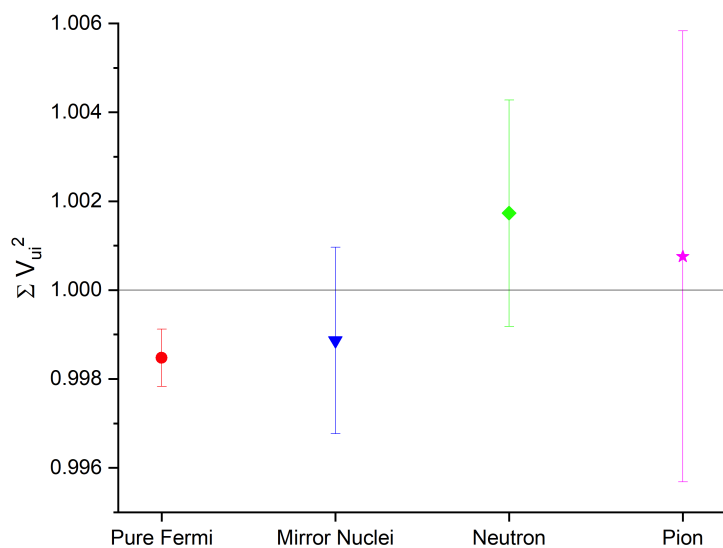


**Figure 1.** The current status of unitarity of the up-quark matrix mixing elements, using  $V_{ud}$  determination from pure Fermi, mixed mirror, neutron, and pion decays. The neutron decay value presented is the global average as reported in [13].

Apart from being an additional precise probe of  $V_{ud}$ , mirror decays can be used to probe various calculation methods of theoretical corrections to  $f_{Vt}$ -values. The validity of models used to determine the isospin symmetry breaking correction ( $\delta_C$ ) was recently reevaluated using tests based on the conserved vector current (CVC) hypothesis and  $f_{Vt}$ -value measurements of superallowed pure Fermi transitions [8]. These tests revealed an inconsistency of the Hartree–Fock (HF) radial wavefunction calculations with the CVC hypothesis, while the  $f_{Vt}$ -value ratio measurements were found to be more consistent with the so-called SM-WS approach of [15], motivating the use of the latter of these calculations for  $\delta_C$  determination. Consequently, this has motivated efforts to both recalculate the radial overlap correction for HF wavefunctions [16] and to calculate  $\delta_C$  using ab initio methods [17–19] and density functional theories [20]. Additional input from mirror decays would be a unique test of the calculation methods currently employed for  $\delta_C$  and would provide future direction for first principles efforts.

Additionally, the current  $2.4\sigma$  deviation from unitarity present in the pure Fermi decay evaluation was revealed in large part due to state-of-the-art calculations of the transition-independent radiative correction ( $\Delta_R$ ) using dispersion relations to calculate the relevant  $\gamma W$ -box corrections [21]. A similar approach is applied to transition-dependent corrections  $\delta_{NS}$  [22], which result in a shift of the corrected  $f_{Vt}$ -value from pure Fermi decays of  $\sim 2\sigma$ . With further developments of these methods underway [23], the additional set of mirror decay  $f_{Vt}$ -values would provide critical validation (or not) of this new approach.

Mirror decays also offer a unique probe of exotic currents beyond the predictions of the Standard Model. While both pure Fermi and mirror decays offer probes of exotic scalar currents, mirror decays also offer a probe of exotic tensor currents [3] and, therefore, offer the best simultaneous constraint on tensor and scalar currents [24]. In the presence of such currents, the right-hand side of Equation (2) is multiplied by the factor [3]:

$$\frac{1}{1 + b_i \langle m_e / E_e \rangle}, \quad (3)$$

where:

$$b_i \langle m_e / E_e \rangle \approx \pm \text{Re} \left( \frac{C_S + C'_S}{C_V + C'_V} \right) C_{SV} \pm \text{Re} \left( \frac{C_T + C'_T}{C_A + C'_A} \right) C_{TA}. \quad (4)$$

Using [25], we can rewrite the multiplicative factors related to the exotic scalar ( $C_{SV}$ ) and tensor ( $C_{TA}$ ) terms that contribute to the corrected  $f_{Vt}$ -values as:

$$C_{SV} = \frac{5\gamma}{1 + \rho^2} \frac{m_e}{Q_{EC} - m_e}, \quad (5)$$

$$C_{TA} = \frac{5\gamma\rho^2}{1 + \rho^2} \frac{m_e}{Q_{EC} - m_e}, \quad (6)$$

where  $m_e$  is the electron mass,  $Q_{EC}$  is the total transition energy of the decay, and  $\gamma = \sqrt{1 - \alpha_{FS}^2 Z^2}$ , where  $\alpha_{FS}$  is the fine-structure constant, and  $Z$  is the proton number. Table 1 shows the calculation results for these factors for mirror and, for comparison, a few pure Fermi and pure Gamow–Teller decays; the greater the factor, the greater the effect from the respective SM-violating current [3]. In particular,  $^{17}\text{F}$  has the largest tensor current factor, comparable in size to that of the  $^6\text{He}$  decay [26].  $^{13}\text{N}$  and  $^{11}\text{C}$  also constrain exotic scalar currents to a comparable level to their  $^{14}\text{O}$  Fermi decaying counterpart. Additionally, constraints on scalar and tensor currents from mirror decays can play a significant role in BSM scenarios involving right-handed neutrinos [24].

**Table 1.** A table of  $\beta$ -emitting nuclei and their sensitivity to exotic scalar and/or tensor currents. Column 1 gives the  $\beta$ -decay mother, and the mixing ratios ( $\rho$ ) as calculated from the SM are shown in Column 2. Columns 3 and 4 give the multiplicative factors for the exotic scalar ( $C_{SV}$ ) and tensor ( $C_{TA}$ ) terms used in the determination of corrected  $f_{Vt}$ -values (more details in [3]). Most shown emitters undergo a superallowed mixed mirror  $\beta$ -decay, except  $^{10}\text{C}$  and  $^{14}\text{O}$ , which decay via a pure Fermi transition, and  $^6\text{He}$ , which decays via a pure Gamow–Teller transition.

| Nuclei           | $\rho$ | $C_{SV}$ | $C_{TA}$ |
|------------------|--------|----------|----------|
| $^6\text{He}$    | –      | –        | 0.852    |
| $^{10}\text{C}$  | –      | 1.827    | –        |
| $^{11}\text{C}$  | –0.754 | 1.106    | 0.630    |
| $^{13}\text{N}$  | –0.560 | 1.137    | 0.356    |
| $^{14}\text{O}$  | –      | 1.099    | –        |
| $^{15}\text{O}$  | 0.630  | 0.814    | 0.323    |
| $^{17}\text{F}$  | 1.296  | 0.423    | 0.710    |
| $^{18}\text{Ne}$ | –      | 0.881    | –        |
| $^{19}\text{Ne}$ | –1.602 | 0.262    | 0.672    |
| $^{21}\text{Na}$ | 0.713  | 0.556    | 0.282    |
| $^{22}\text{Mg}$ | –      | 0.704    | –        |
| $^{23}\text{Mg}$ | –0.554 | 0.549    | 0.169    |
| $^{25}\text{Al}$ | 0.808  | 0.408    | 0.267    |
| $^{27}\text{Si}$ | –0.697 | 0.398    | 0.193    |
| $^{29}\text{P}$  | 0.538  | 0.444    | 0.129    |
| $^{31}\text{S}$  | –0.529 | 0.406    | 0.114    |
| $^{33}\text{Cl}$ | –0.314 | 0.455    | 0.045    |
| $^{35}\text{Ar}$ | 0.282  | 0.430    | 0.034    |
| $^{37}\text{K}$  | –0.578 | 0.337    | 0.112    |
| $^{39}\text{Ca}$ | 0.661  | 0.293    | 0.128    |
| $^{41}\text{Sc}$ | 1.074  | 0.196    | 0.226    |
| $^{43}\text{Ti}$ | –0.810 | 0.239    | 0.157    |
| $^{45}\text{V}$  | 0.635  | 0.272    | 0.109    |

Despite the clear need for data, the list of mirror decays where all necessary experimental quantities are currently precisely measured comprises only five transitions:  $^{19}\text{Ne}$ ,  $^{21}\text{Na}$ ,  $^{29}\text{P}$ ,  $^{35}\text{Ar}$ , and  $^{37}\text{K}$  [11] due to the difficulty in measuring the extra piece not required for their pure Fermi transition counterparts: the mixing ratio ( $\rho$ ). In lieu of a clear need for more measurements, recent [27] and planned experiments [28,29] have taken aim at measuring this mixing ratio for a few transitions already part of the aforementioned list.

Therefore, they do not span the number of transitions needed to sufficiently improve the overall precision on the corrected mirror  $f_{\nu t}$ -value. To remedy the absence of the needed measurements, the Superallowed Transition Beta-Neutrino Ion Coincidence Trap (St. Benedict) is currently under construction at the University of Notre Dame's Nuclear Science Laboratory (NSL), with the aim of measuring  $\rho$  for a wide range of superallowed mirror decays between  $^{11}\text{C}$  and  $^{41}\text{Sc}$  [30]. With a wide range of high-rate near-stability radioactive ion beams (RIBs) and ample availability, the *TwinSol* facility at the NSL provides a perfect space to probe a swath of mirror transitions, positioning St. Benedict to have a critical role in testing the Standard Model via superallowed mirror decays. The rest of this article is ordered as follows: we first present the method by which St. Benedict will determine the  $\rho$ , as well as the elements required to prepare and measure this quantity in radioactive isotopes at the NSL. Secondly, we detail the results of simulations in advance of the first measurements at the facility. Finally, we touch on future developments planned at the NSL to provide further interesting RIBs to the St. Benedict facility.

## 2. Materials and Methods

St. Benedict will be coupled with the *TwinSol* facility [31], which enables production and separation of in-flight RIBs, in part due to two superconducting solenoids. The facility has had a history of success producing light-to-medium mass RIBs a few nucleons away from stability [32,33], including many of the mirror nuclei relevant for measurement [34–37]. The St. Benedict facility will consist of four distinct elements for beam preparation, manipulation, and measurement, all of which are either commissioned or currently being constructed. A schematic of the St. Benedict facility is shown in Figure 2. A large-volume gas catcher will be used to thermalize high-energy ( $\sim 10\text{--}40$  MeV) beams from *TwinSol*, accomplished via a degrader to adjust the range of the incident radioactive ions and flowing ultra-high purity He gas for stopping. The gas catcher has been previously used at Argonne National Laboratory and has been recommissioned at the NSL with an offline source. Thermalized beams will exit the gas catcher and be collected by an RF carpet, a 2D trapping device that guides ions parallel to its surface towards a central aperture via RF fields, and is ideal for beam transport at pressures above 1 mbar [38,39]. Once collected, the beams are transported by an RFQ ion guide to an RFQ cooler-buncher [40], which will reduce the beam emittance via collisions with a He buffer gas and bunch beams into discrete ion bunches for efficient injection into a measurement Paul trap [41]. The Paul trap electrode rods are made of a low-porosity graphite, a low-Z material that helps minimize  $\beta$ -scattering, an otherwise dominant systematic. Other systematic effects, such as uncertainties due to the ion cloud size and the RF effects on ion trajectories, are expected to contribute at below the 0.5% level. More on the various elements of the St. Benedict system can be found in [42].

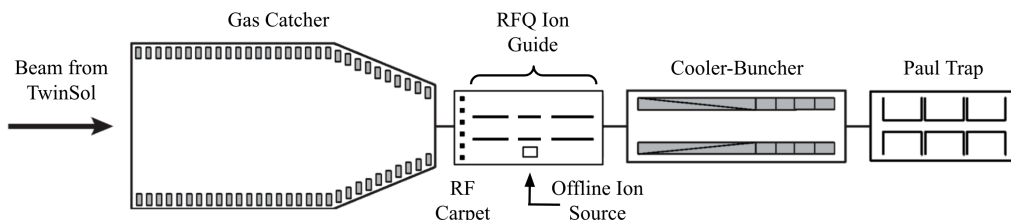


**Figure 2.** A schematic of the primary trapping components of the St. Benedict facility. Radioactive ion beams will enter the gas catcher from *TwinSol* and will progress through each component before measurement in the Paul trap. Two DSSDs and two MCPs, which are not pictured, surround the Paul trap parallel to the incoming beam.

Mixing ratios will be determined via measurement of the beta-neutrino angular correlation parameter ( $a_{\beta\nu}$ ) of mirror nuclides in a Paul trap. A recent study of angular correlations in beta decays showed that  $a_{\beta\nu}$  offers a greater sensitivity to  $\rho$  than other measurable quantities, most notably the beta-asymmetry parameter ( $A_\beta$ ), for a number

of light mirror nuclei [43]. In Table 2, we present the results of an expanded and updated sensitivity study that includes all potential mirror nuclei measurements at St. Benedict and the newest calculated values of  $\rho$  reported in [44]. Of the 20 nuclei studied, 16 of them have a mixing ratio that is more sensitive to a measurement of  $a_{\beta\nu}$  than  $A_\beta$ . Assuming relative precisions of 0.5% on the  $A_\beta$  and  $a_{\beta\nu}$  measurements, the resulting average relative precision on  $\rho$  is 3.4% and 0.63%, respectively. This indicates that a determination of  $\rho$  is, on average, about 5 times more sensitive to a measurement of  $a_{\beta\nu}$  versus  $A_\beta$  given precisions purely from statistical uncertainties.

**Table 2.** A table of mirror nuclei and the sensitivity of  $\rho$  to  $a_{\beta\nu}$  and  $A_\beta$ . Column 1 gives the  $\beta$ -decay mother, and the mixing ratios ( $\rho$ ) are shown in Column 2. Columns 3 and 5 give the multiplicative factors  $F_A$  and  $F_a$  such that  $\frac{\delta A_\beta}{A_\beta} = F_A \frac{\delta \rho}{\rho}$  and  $\frac{\delta a_{\beta\nu}}{a_{\beta\nu}} = F_a \frac{\delta \rho}{\rho}$ , respectively. Columns 4 and 6 give values for the relative precision on  $\rho$  if  $\frac{\delta A_\beta}{A_\beta}$  or  $\frac{\delta a_{\beta\nu}}{a_{\beta\nu}}$  is 0.5%, respectively. All relative precisions are reported as percentages.

| Nuclei           | $\rho$ | Sensitivity to $a_{\beta\nu}$ | $\delta \rho / \rho$ from $a_{\beta\nu}$ | Sensitivity to $A_\beta$ | $\delta \rho / \rho$ from $A_\beta$ |
|------------------|--------|-------------------------------|--|--------------------------|-------------------------------------|
| $n$              | 2.218  | 3.52                          | 0.14                                     | -0.10                    | 5.03                                |
| $^3\text{H}$     | -2.105 | 4.63                          | 0.11                                     | 5.08                     | 0.10                                |
| $^{11}\text{C}$  | -0.754 | -1.19                         | 0.42                                     | 0.03                     | 14.99                               |
| $^{13}\text{N}$  | -0.560 | -0.70                         | 0.71                                     | 0.05                     | 9.54                                |
| $^{15}\text{O}$  | 0.630  | -0.87                         | 0.57                                     | 0.70                     | 0.72                                |
| $^{17}\text{F}$  | 1.296  | -3.80                         | 0.13                                     | -0.07                    | 6.76                                |
| $^{19}\text{Ne}$ | -1.602 | -13.28                        | 0.04                                     | -12.76                   | 0.04                                |
| $^{21}\text{Na}$ | 0.713  | -1.08                         | 0.46                                     | 0.48                     | 1.04                                |
| $^{23}\text{Mg}$ | -0.554 | -0.70                         | 0.72                                     | 0.36                     | 1.38                                |
| $^{25}\text{Al}$ | 0.808  | -1.35                         | 0.37                                     | 0.33                     | 1.51                                |
| $^{27}\text{Si}$ | -0.697 | -1.04                         | 0.48                                     | 0.21                     | 2.35                                |
| $^{29}\text{P}$  | 0.538  | -0.66                         | 0.75                                     | 0.79                     | 0.63                                |
| $^{31}\text{S}$  | -0.529 | -0.64                         | 0.78                                     | 0.12                     | 4.07                                |
| $^{33}\text{Cl}$ | -0.314 | -0.25                         | 2.02                                     | 0.73                     | 0.68                                |
| $^{35}\text{Ar}$ | 0.282  | -0.20                         | 2.48                                     | 0.92                     | 0.54                                |
| $^{37}\text{K}$  | -0.578 | -0.75                         | 0.67                                     | 0.32                     | 1.54                                |
| $^{39}\text{Ca}$ | 0.660  | -0.95                         | 0.53                                     | 0.54                     | 0.93                                |
| $^{41}\text{Sc}$ | 1.074  | -2.32                         | 0.22                                     | 0.05                     | 10.49                               |
| $^{43}\text{Ti}$ | -0.810 | -1.35                         | 0.37                                     | 0.09                     | 5.32                                |
| $^{45}\text{V}$  | 0.635  | -0.89                         | 0.56                                     | 0.50                     | 1.00                                |

The St. Benedict measurement Paul trap consists of four rods segmented into three sets of electrodes. Confinement is achieved by a radio-frequency (RF) field applied together with static DC voltages on the rods. Mother ions are injected into the Paul trap and recooled via collisions with a high-purity He buffer gas at  $\sim 10^{-6}$  torr. Confined mother ions decay after some time in the trap, and the recoiling daughter ions are detected by one of two micro-channel plate (MCP) detectors, which records the time and position of an ion hit.  $\beta$ -particles from the decay are detected by one of two double-sided silicon strip detectors (DSSDs) for position readout.  $\beta$ s are subsequently stopped in a large-volume plastic scintillator placed directly behind the DSSDs for timing readout. The distribution of differences in detection times between a  $\beta$ -particle and a daughter ion (referred to from here forward as the time-of-flight) is used to extract the beta-neutrino angular correlation parameter [45].

### 3. Results

In order to determine the feasibility of  $a_{\beta\nu}$  measurements with St. Benedict at the *TwinSol* facility, a series of simulations have been completed. Using both SIMION [46] and Geant4 [47], the trajectories of decayed daughter ions were simulated, within a time-varying electric field at a realistic trapping frequency. The initial positions and momenta of the

decayed ions were determined by sampling from the differential rate in [48], and the subsequent time-of-flight of ions that impact an MCP detector were recorded. Because the time-of-flight distribution varies linearly with  $a_{\beta\nu}$ , a linear combination of simulated distributions with different  $a_{\beta\nu}$ , labeled  $a_1$  and  $a_2$ , are fit to the experimental time-of-flight data to extract  $a_{\beta\nu}$ , similar to the method of [49]. This linear combination is given as:

$$\beta(\alpha F_{a1}(t) + (1 - \alpha)F_{a2}(t)), \quad (7)$$

where  $F_{a1}(t)$  and  $F_{a2}(t)$  are the two additional time-of-flight distributions for  $a_1$  and  $a_2$ , respectively, and  $\beta$  and  $\alpha$  are the fit parameters.  $a_{\beta\nu}$  is determined from  $\alpha$  by:

$$a_{\beta\nu} = \alpha a_1 + (1 - \alpha) a_2. \quad (8)$$

A plot of the fitted simulation results for the decay of  $^{17}\text{F}$  is shown in Figure 3. Using these results, the number of counts required to achieve a statistical uncertainty, which yields a relative precision of 0.5% and 0.1% was established. Combining this result with the established *TwinSol* production rates and  $\beta$ -decay half-lives gives estimates for beamtime days required to complete a measurement to the desired precision. These results are shown in Figure 4. In all cases, the time required for background measurement and injected ion bunch cooling is considered. Mirrors that do not have associated bars do not have established production rates from *TwinSol*.

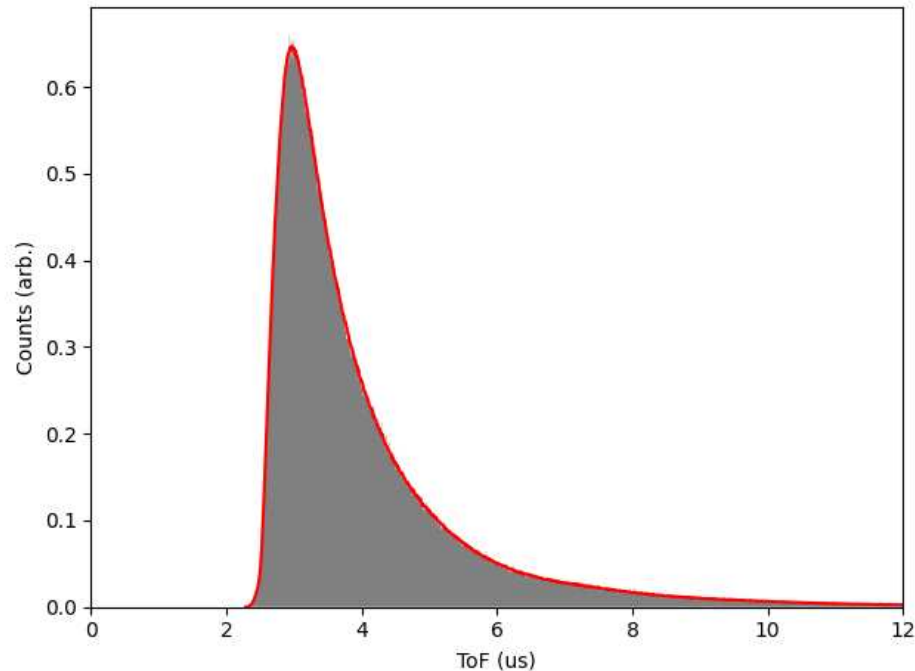


**Figure 3.** A plot of times of flight of simulated  $^{17}\text{O}$  daughter ions inside the St. Benedict measurement Paul trap. The result of fitting Equation (7) is shown in red. Ten million daughter ions were simulated in this example.

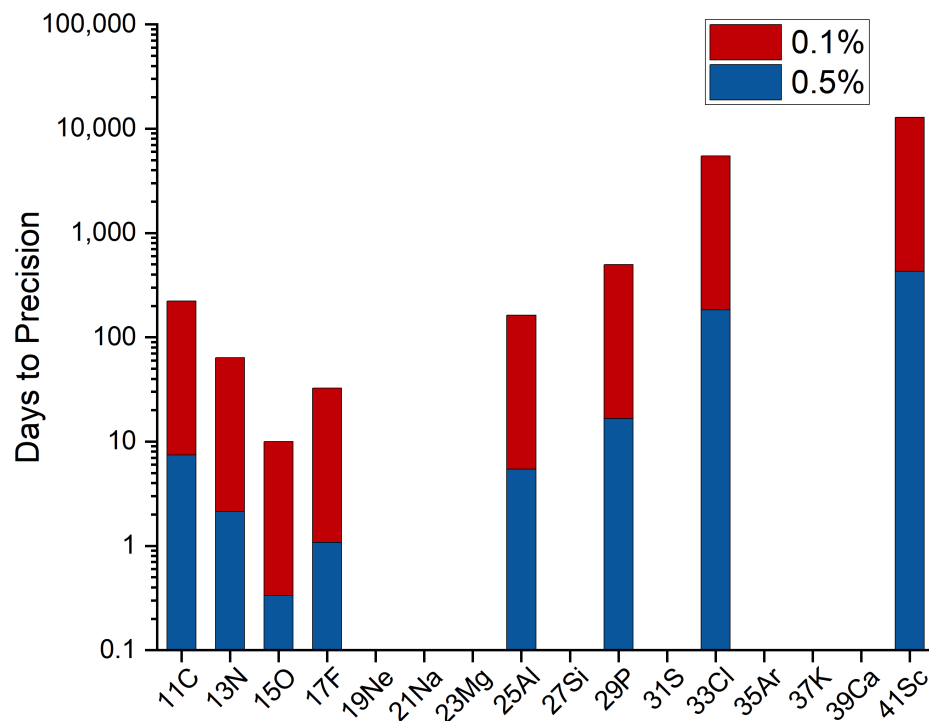


**Figure 4.** A chart of the radioactive beamtime days required to achieve the desired relative precisions on  $a_{\beta\nu}$  at the *TwinSol* facility. Blue bars indicate the time needed to reach 0.5% precision, while red bars indicate the extra time needed to achieve 0.1% precision. Mirror nuclei without any bars do not have established production rates at *TwinSol*.

#### 4. Discussion

Of the relevant mirror nuclei presented in Table 2, eight have experimentally confirmed production rates from *TwinSol*. For the five lightest of these mirrors, the results in Figure 4 indicate a 0.5% precision is achievable in  $\sim 7$  days of beam delivery. Of these light  $\beta$ -emitting mirrors,  $^{17}\text{F}$  is proposed as the flagship measurement for St. Benedict, due to its high production rate ( $\sim 10^6$  pps) and high sensitivity to  $\rho$  (second highest of the potential St. Benedict measurement candidates). Additionally, the highest precision on  $\rho$  for  $^{17}\text{F}$ , stemming from global fits to corrected  $f_V t$ -value data assuming the validity of the Standard Model, is an order of magnitude more precise than results from low-precision data [24], indicating a significant need for high-precision data on  $^{17}\text{F}$  for any robust tests of CKM unitarity.

In the case of mirrors heavier than  $^{29}\text{P}$  and those for which no *TwinSol* rates are established, further beam development is needed to achieve the desired relative uncertainties. The case of  $^{19}\text{Ne}$  is particularly tantalizing due its large sensitivity to  $\rho$  [50]. Beam developments at the NSL and the *TwinSol* facility are planned to make such a measurement possible with St. Benedict. In particular, preliminary calculations in LISE++ [51] indicate that improvements in the beam rate up to an order of magnitude are possible.

#### 5. Conclusions

More precise data are needed on superallowed mixed mirror  $\beta$ -decays given the suite of tests of fundamental symmetries they would enable. The St. Benedict facility is poised to deliver a swath of these data, through precision measurements of the beta-neutrino angular correlation parameter to a relative precision of 0.5%. With a wide range of mirror nuclides available via the *TwinSol* facility at the NSL, St. Benedict aims to posit mirror decays as a probe of CKM unitarity and beyond.

**Author Contributions:** Conceptualization, M.B., P.D.O., D.W.B., J.A.C. and G.S.; Data curation, W.S.P., A.T.G., J.J.K. and C.Q.; Formal analysis, W.S.P.; Funding acquisition, M.B. and D.W.B.; Investigation, W.S.P., M.B., D.P.B., A.T.G., A.M.H., B.L., C.Q., F.R., A.A.V. and R.Z.; Methodology, W.S.P., A.T.G. and M.B.; Project administration, M.B.; Software, A.T.G. and W.S.P.; Supervision, M.B. and A.T.G.; Visualization, W.S.P. and M.B.; Writing—original draft, W.S.P. All authors have read and reviewed this manuscript, and agreed to the published version.

**Funding:** This work was conducted with the support of the University of Notre Dame, the U.S. National Science Foundation under grant numbers PHY-1725711 and PHY-2011890, under the auspices of the U.S. Department of Energy by Lawrence Livermore National Laboratory under Contract DE-AC52-07NA27344, and was supported by the LLNL-LDRD Program under Project No. 19-ERD-011.

**Data Availability Statement:** Data will be made available upon request to the authors. The authors encourage interested readers to reach out to them via email.

**Acknowledgments:** The authors would like to acknowledge the support of the Notre Dame Center for Research Computing in the completion of simulations and analysis.

**Conflicts of Interest:** The authors declare that they have no known competing financial interest, personal relationship, or conflict of interest that could have appeared to influence the work reported in this paper.

## References

1. Lagouri, T. Review on Higgs Hidden–Dark Sector Physics at High-Energy Colliders. *Symmetry* **2022**, *14*, 1299. [\[CrossRef\]](#)
2. Herczeg, P. Beta decay beyond the standard model. *Prog. Part. Nucl. Phys.* **2001**, *46*, 413–457. [\[CrossRef\]](#)
3. González-Alonso, M.; Naviliat-Cuncic, O.; Severijns, N. New physics searches in nuclear and neutron  $\beta$  decay. *Prog. Part. Nucl. Phys.* **2019**, *104*, 165–223.
4. Seng, C.Y. Towards a discovery of BSM physics from the Cabibbo angle anomaly. *Mod. Phys. Lett. A* **2022**, *37*, 2230002. [\[CrossRef\]](#)
5. Towner, I.S.; Hardy, J.C. The evaluation of  $V_{ud}$  and its impact on the unitarity of the Cabibbo–Kobayashi–Maskawa quark-mixing matrix. *Rep. Prog. Phys.* **2010**, *73*, 46301. [\[CrossRef\]](#)
6. Blucher, E.; Marciano, W.  $V_{ud}, V_{us}$ , the Cabibbo Angles, and CKM Unitarity; Minireview for the Particle Data Group: 2019; pp. 1–10.
7. Tanabashi, M.  $V_{cb}$  and  $V_{ub}$  CKM Matrix Elements. *Phys. Rev.* **2018**, *98*, 030001.
8. Hardy, J.C.; Towner, I.S. Superallowed  $0^+ \rightarrow 0^+$  nuclear  $\beta$  decays: 2020 critical survey, with implications for  $V_{ud}$  and CKM unitarity. *Phys. Rev. C* **2020**, *102*, 45501. [\[CrossRef\]](#)
9. Počanić, D.; Frlež, E.; Baranov, V.A.; Bertl, W.; Brönnimann, C.; Bychkov, M.; Crawford, J.F.; Daum, M.; Khomutov, N.V.; Korenchenko, A.S.; et al. Precise Measurement of the  $\pi^+ \rightarrow \pi^0 e^+ \nu$  Branching Ratio. *Phys. Rev. Lett.* **2004**, *93*, 181803. [\[CrossRef\]](#)
10. Czarnecki, A.; Marciano, W.J.; Sirlin, A. Neutron Lifetime and Axial Coupling Connection. *Phys. Rev. Lett.* **2018**, *120*, 202002. [\[CrossRef\]](#)
11. Naviliat-Cuncic, O.; Severijns, N. Test of the Conserved Vector Current Hypothesis in  $T = 1/2$  Mirror Transitions and New Determination of  $|V_{ud}|$ . *Phys. Rev. Lett.* **2009**, *102*, 142302. [\[CrossRef\]](#)
12. Severijns, N.; Tandecki, M.; Phalet, T.; Towner, I.S.  $\mathcal{F}t$  values of the  $T = 1/2$  mirror  $\beta$  transitions. *Phys. Rev. C* **2008**, *78*, 55501. [\[CrossRef\]](#)
13. Hardy, J.C.; Towner, I.S. Nuclear beta decays and CKM unitarity. *arXiv* **2018**, arXiv:1807.01146.
14. Falkowski, A.; González-Alonso, M.; Naviliat-Cuncic, O.; Severijns, N. Superallowed decays within and beyond the standard model. *Eur. Phys. J. A* **2023**, *59*, 113. [\[CrossRef\]](#)
15. Towner, I.S.; Hardy, J.C. Improved calculation of the isospin-symmetry-breaking corrections to superallowed Fermi  $\beta$  decay. *Phys. Rev. C* **2008**, *77*, 25501. [\[CrossRef\]](#)
16. Xayavong, L.; Smirnova, N.A. Radial overlap correction to superallowed  $0^+ \rightarrow 0^+$  nuclear  $\beta$  decays using the shell model with Hartree-Fock radial wave functions. *Phys. Rev. C* **2022**, *105*, 44308. [\[CrossRef\]](#)
17. Stroberg, S.R. Beta Decay in Medium-Mass Nuclei with the In-Medium Similarity Renormalization Group. *Particles* **2021**, *4*, 521–535.
18. Martin, M.S.; Stroberg, S.R.; Holt, J.D.; Leach, K.G. Testing isospin symmetry breaking in ab initio nuclear theory. *Phys. Rev. C* **2021**, *104*, 14324. [\[CrossRef\]](#)
19. Seng, C.Y.; Gorchtein, M. Towards *ab-initio* nuclear theory calculations of  $\delta_C$ . *arXiv* **2023**, arXiv:2304.03800.
20. Konieczka, M.; Bączyk, P.; Satuła, W. Precision calculation of isospin-symmetry-breaking corrections to  $T = 1/2$  mirror decays using configuration-interaction framework built upon multireference charge-dependent density functional theory. *Phys. Rev. C* **2022**, *105*, 65505. [\[CrossRef\]](#)
21. Seng, C.Y.; Gorchtein, M.; Patel, H.H.; Ramsey-Musolf, M.J. Reduced Hadronic Uncertainty in the Determination of  $V_{ud}$ . *Phys. Rev. Lett.* **2018**, *121*, 241804. [\[CrossRef\]](#)
22. Seng, C.Y.; Gorchtein, M. Dispersive formalism for the nuclear structure correction  $\delta_{NS}$  to the  $\beta$  decay rate. *Phys. Rev. C* **2023**, *107*, 035503. [\[CrossRef\]](#)

23. Seng, C.Y.; Gorchtein, M.; Ramsey-Musolf, M.J. Dispersive evaluation of the inner radiative correction in neutron and nuclear  $\beta$  decay. *Phys. Rev. D* **2019**, *100*, 13001. [\[CrossRef\]](#)

24. Falkowski, A.; González-Alonso, M.; Naviliat-Cuncic, O. Comprehensive analysis of beta decays within and beyond the Standard Model. *J. High Energy Phys.* **2021**, *2021*, 126. [\[CrossRef\]](#)

25. Towner, I.S.; Hardy, J.C. Parametrization of the statistical rate function for select superallowed transitions. *Phys. Rev. C* **2015**, *91*, 015501. [\[CrossRef\]](#)

26. Naviliat-Cuncic, O.; Ban, G.; Dur, D.; Duval, F.; Fléchard, X.; Herbane, M.; Labalme, M.; Liénard, E.; Mauger, F.; Mery, A.; et al. Measurement of the electron-neutrino angular correlation in  ${}^6\text{He}$  decay. *AIP Conf. Proc.* **2006**, *870*, 291–294. [\[CrossRef\]](#)

27. Liénard, E.; Ban, G.; Couratin, C.; Delahaye, P.; Durand, D.; Fabian, X.; Fabre, B.; Fléchard, X.; Finlay, P.; Mauger, F.; et al. Precision measurements with LPCTrap at GANIL. *Hyperfine Interact.* **2015**, *236*, 1–7. [\[CrossRef\]](#)

28. Ohayon, B.; Chocron, J.; Hirsh, T.; Glick-Magid, A.; Mishnayot, Y.; Mukul, I.; Rahangdale, H.; Vaintraub, S.; Heber, O.; Gazit, D.; et al. Weak interaction studies at SARAF. *Hyperfine Interact.* **2018**, *239*, 57. [\[CrossRef\]](#)

29. Fenker, B.; Gorelov, A.; Melconian, D.; Behr, J.; Anholm, M.; Ashery, D.; Behling, R.; Cohen, I.; Craiciu, I.; Gwinner, G.; et al. Precision Measurement of the  $\beta$  Asymmetry in Spin-Polarized  ${}^{37}\text{K}$  Decay. *Phys. Rev. Lett.* **2018**, *120*, 62502. [\[CrossRef\]](#)

30. O’Malley, P.D.; Brodeur, M.; Burdette, D.P.; Klimes, J.W.; Valverde, A.A.; Clark, J.A.; Savard, G.; Ringle, R.; Varentsov, V. Testing the weak interaction using St. Benedict at the University of Notre Dame. *Nucl. Instrum. Methods Phys. Res. Sect. B Beam Interact. Mater. Atoms* **2020**, *463*, 488–490. [\[CrossRef\]](#)

31. Beccetti, F.D.; Lee, M.Y.; O’Donnell, T.W.; Roberts, D.A.; Kolata, J.J.; Lamm, L.O.; Rogachev, G.; Guimarães, V.; DeYoung, P.A.; Vincent, S. The TwinSol low-energy radioactive nuclear beam apparatus: status and recent results. *Nucl. Instrum. Methods Phys. Res. Sect. A Accel. Spectrom. Detect. Assoc. Equip.* **2003**, *505*, 377–380. [\[CrossRef\]](#)

32. Aguilera, E.F.; Amador-Valenzuela, P.; Martinez-Quiroz, E.; Lizcano, D.; Rosales, P.; García-Martínez, H.; Gómez-Camacho, A.; Kolata, J.J.; Roberts, A.; Lamm, L.O.; et al. Near-Barrier Fusion of the  ${}^8\text{B} + {}^{58}\text{Ni}$  Proton-Halo System. *Phys. Rev. Lett.* **2011**, *107*, 92701. [\[CrossRef\]](#)

33. Henderson, S.L.; Ahn, T.; Caprio, M.A.; Fasano, P.J.; Simon, A.; Tan, W.; O’Malley, P.; Allen, J.; Bardayan, D.W.; Blankstein, D.; et al. First measurement of the  $B(E2; 3/2^- \rightarrow 1/2^-)$  transition strength in  ${}^7\text{Be}$ : Testing *ab initio* predictions for  $A = 7$  nuclei. *Phys. Rev. C* **2019**, *99*, 64320. [\[CrossRef\]](#)

34. Brodeur, M.; Nicoloff, C.; Ahn, T.; Allen, J.; Bardayan, D.W.; Beccetti, F.D.; Gupta, Y.K.; Hall, M.R.; Hall, O.; Hu, J.; et al. Precision half-life measurement of  ${}^{17}\text{F}$ . *Phys. Rev. C* **2016**, *93*, 25503. [\[CrossRef\]](#)

35. Burdette, D.P.; Brodeur, M.; Bardayan, D.W.; Beccetti, F.D.; Blankstein, D.; Boomershine, C.; Caves, L.; Henderson, S.L.; Kolata, J.J.; Liu, B.; et al. Precise half-life determination of the mixed-mirror  $\beta$ -decaying  ${}^{15}\text{O}$ . *Phys. Rev. C* **2020**, *101*, 55504. [\[CrossRef\]](#)

36. Long, J.; Nicoloff, C.R.; Bardayan, D.W.; Beccetti, F.D.; Blankstein, D.; Boomershine, C.; Burdette, D.P.; Caprio, M.A.; Caves, L.; Fasano, P.J.; et al. Precision half-life determination for the  $\beta^+$  emitter  ${}^{13}\text{N}$ . *Phys. Rev. C* **2022**, *106*, 45501. [\[CrossRef\]](#)

37. Valverde, A.A.; Brodeur, M.; Ahn, T.; Allen, J.; Bardayan, D.W.; Beccetti, F.D.; Blankstein, D.; Brown, G.; Burdette, D.P.; Frentz, B.; et al. Precision half-life measurement of  ${}^{11}\text{C}$ : The most precise mirror transition  $\mathcal{F}t$  value. *Phys. Rev. C* **2018**, *97*, 35503. [\[CrossRef\]](#)

38. Davis, C.; Bruce, O.; Burdette, D.P.; Florenzo, T.; Liu, B.; Long, J.; O’Malley, P.D.; Yeck, M.A.; Brodeur, M. Transport tests of the St. Benedict first-stage extraction system. *Nucl. Instrum. Methods Phys. Res. Sect. A Accel. Spectrom. Detect. Assoc. Equip.* **2022**, *1031*, 166509. [\[CrossRef\]](#)

39. Davis, C.; Bualuan, R.; Bruce, O.; Burdette, D.P.; Cannon, A.; Florenzo, T.; Gan, D.; Harkin, J.; Liu, B.; Long, J.; et al. Commissioning of the St. Benedict RF carpet. *Nucl. Instrum. Methods Phys. Res. Sect. A Accel. Spectrom. Detect. Assoc. Equip.* **2022**, *1042*, 167422. [\[CrossRef\]](#)

40. Valverde, A.A.; Brodeur, M.; Burdette, D.P.; Clark, J.A.; Klimes, J.W.; Lascar, D.; O’Malley, P.D.; Ringle, R.; Savard, G.; Varentsov, V. Stopped, bunched beams for the TwinSol facility. *Hyperfine Interact.* **2019**, *240*, 38. [\[CrossRef\]](#)

41. Burdette, D.; Brodeur, M.; O’Malley, P.; Valverde, A. Development of the St. Benedict Paul Trap at the Nuclear Science Laboratory. *Hyperfine Interact.* **2019**, *240*, 70. [\[CrossRef\]](#)

42. Brodeur, M.; Ahn, T.; Bardayan, D.W.; Burdette, D.P.; Clark, J.A.; Gallant, A.T.; Kolata, J.J.; Liu, B.; O’Malley, P.D.; Porter, W.S.; et al. Construction of St. Benedict. *Nucl. Instrum. Methods Phys. Res. Sect. B Beam Interact. Mater. Atoms* **2023**, *541*, 79–81. [\[CrossRef\]](#)

43. Hayen, L.; Young, A.R. Consistent description of angular correlations in  $\beta$  decay for Beyond Standard Model physics searches. *arXiv* **2020**, arXiv:2009.11364.

44. Severijns, N.; Hayen, L.; De Leebeeck, V.; Vanlangendonck, S.; Bodek, K.; Rozpedzik, D.; Towner, I.S.  $\mathcal{F}t$  values of the mirror  $\beta$  transitions and the weak-magnetism-induced current in allowed nuclear  $\beta$  decay. *Phys. Rev. C* **2023**, *107*, 15502. [\[CrossRef\]](#)

45. Fléchard, X.; Liénard, E.; Méry, A.; Rodríguez, D.; Ban, G.; Durand, D.; Duval, F.; Herbane, M.; Labalme, M.; Mauger, F.; et al. Paul Trapping of Radioactive  ${}^6\text{He}^+$  Ions and Direct Observation of Their  $\beta$  Decay. *Phys. Rev. Lett.* **2008**, *101*, 212504. [\[CrossRef\]](#) [\[PubMed\]](#)

46. Dahl, D.A. SIMION for the personal computer in reflection. *Int. J. Mass Spectrom.* **2000**, *200*, 3–25. [\[CrossRef\]](#)

47. Agostinelli, S.; Allison, J.; Amako, K.; Apostolakis, J.; Araujo, H.; Arce, P.; Asai, M.; Axen, D.; Banerjee, S.; Barrand, G.; et al. Geant4—A simulation toolkit. *Nucl. Instrum. Methods Phys. Res. Sect. A Accel. Spectrom. Detect. Assoc. Equip.* **2003**, *506*, 250–303. [\[CrossRef\]](#)

48. Holstein, B.R. Recoil effects in allowed beta decay: The elementary particle approach. *Rev. Mod. Phys.* **1974**, *46*, 789–814. [[CrossRef](#)]
49. Ban, G.; Durand, D.; Fléchard, X.; Liénard, E.; Naviliat-Cuncic, O. Precision measurements in nuclear  $\beta$ -decay with LPCTrap. *Ann. Phys.* **2013**, *525*, 576–587. [[CrossRef](#)]
50. Ohayon, B.; Rahangdale, H.; Parnes, E.; Perelman, G.; Heber, O.; Ron, G. Decay microscope for trapped neon isotopes. *Phys. Rev. C* **2020**, *101*, 35501. [[CrossRef](#)]
51. Tarasov, O.; Bazin, D. LISE++: Exotic beam production with fragment separators and their design. *Nucl. Instrum. Methods Phys. Res. Sect. B Beam Interact. Mater. Atoms* **2016**, *376*, 185–187.

**Disclaimer/Publisher’s Note:** The statements, opinions and data contained in all publications are solely those of the individual author(s) and contributor(s) and not of MDPI and/or the editor(s). MDPI and/or the editor(s) disclaim responsibility for any injury to people or property resulting from any ideas, methods, instructions or products referred to in the content.